remote sensing

IMPACT FACTOR 5.349

CITESCORE 7.4

Article

Comparison of Normalized Difference Vegetation Index Derived from Landsat, MODIS, and AVHRR for the Mesopotamian Marshes Between 2002 and 2018

Reyadh Albarakat and Venkataraman Lakshmi

MDPI

https://doi.org/10.3390/rs11101245

remote sensing

MDPI

Article

Comparison of Normalized Difference Vegetation Index Derived from Landsat, MODIS, and AVHRR for the Mesopotamian Marshes Between 2002 and 2018

Reyadh Albarakat [1,*] and Venkataraman Lakshmi [2]

[1] Ocean and Environment, School of Earth, University of South Carolina, Columbia, SC 29208, USA
[2] Engineering Systems and Environment, University of Virginia Charlottesville, Charlottesville, VA 22904, USA; vlakshmi@virginia.edu
* Correspondence: ralbarakat@geol.sc.edu

Received: 21 April 2019; Accepted: 22 May 2019; Published: 25 May 2019

Abstract: The Mesopotamian marshes are a group of water bodies located in southern Iraq, in the shape of a triangle, with the cities Amarah, Nasiriyah, and Basra located at its corners. The marshes are appropriate habitats for a variety of birds and most of the commercial fisheries in the region. The normalized difference vegetation index (NDVI) has been derived using observations from various satellite sensors, such as the Moderate Resolution Imaging Spectroradiometer (MODIS), Advanced Very-High-Resolution Radiometer (AVHRR), and Landsat over the Mesopotamian marshlands for the 17-year period between 2002 and 2018. We have chosen this time series (2002–2018) to monitor the change in vegetation of the study area since it is considered as a period of rehabilitation for the marshes (following a period when there was little to no water flowing into the marshes). Statistical analyses were performed to monitor the variability of the maximum biomass time (month of June). The results illustrated a strong positive correlation between the NDVI derived from Landsat, MODIS, and AVHRR. The statistical correlations were 0.79, 0.77, and 0.96 between Landsat and AVHRR, MODIS and AVHRR, and Landsat and MODIS, respectively. The linear slope of NDVI (Landsat, MODIS, and AVHRR) for each pixel over the period 2002–2018 displays a long-term trend of green biomass (NDVI) change in the study area, and the slope is slightly negative over most of the area. Slope values (−0.002 to −0.05) denote a slight decrease in the observed vegetation index over 17 years. The green biomass of the marshlands increased by 33.2% of the total area over 17 years. The areas of negative and positive slopes correspond to the same areas in slope map when calculated from Landsat, MODIS, and AVHRR, although they are different in spatial resolution (30 m, 1 km, and 5 km, respectively). The time series of the average NDVI (2002–2018) for three different sensors shows the highest and lowest NDVI values during the same years (for the month of June each year). The highest values were 0.19, 0.22, and 0.22 for Landsat, MODIS, and AVHRR, respectively, in 2006, and the lowest values were 0.09, 0.14, and 0.09 for Landsat, MODIS, and AVHRR, respectively, in 2003.

Keywords: sensors; remote sensing; comparison; Iraq; NDVI; AVHRR; MODIS; Landsat

1. Introduction

The Mesopotamian marshes in Iraq are regarded as one of the most vital wetlands in the world. It is the largest ecosystem in the Middle East and western Asia. During the previous few decades, the area of marshlands has varied between 10,500 km^2 and 20,000 km^2 due to flooding. The marshlands include the Al Hammar marsh, the Central marshes or Al-Amarah marsh, and the Al-Huwaiza marsh [1,2]. The marshes are a source of biodiversity in the Middle East, because of their size, hydrous vegetation, and their detachment from comparative equivalent frameworks [3,4]. The quick drying up of more than

10,000 km^2 of wetlands and lakes will undoubtedly have noteworthy consequences on the atmosphere at a local scale. If the wetlands are eliminated, evapotranspiration and moistness rates will diminish, and precipitation patterns will change as well [5]. Temperatures will rise, especially during the long summers, with strong and dry winds and temperatures rising to more than 40 °C [6]. However, these areas suffer from numerous problems [5]. Biological system decay has an impact on human health, including water shortage and contamination from harmful dust storms blowing off saltpans and dried swamp beds.

The marshlands were subjected to drying operations from the late 1980s to late 2003 because of the anthropogenic activities of the river damming operations upstream, which were politically-driven and caused an ecological disaster in the region [2,7]. The degradation was a decline in the area of vegetation and a conversion into barren land. It is worth mentioning that the Mesopotamian marshlands experienced re-flooding in late 2003 after the fall of Saddam's regime, due to the return of marsh dwellers, who destroyed many of the canals and dams that had been built and restoring flow to the marshes.

Satellite datasets have been widely utilized to monitor the changes in vegetation coverage. An assessment of temporal changes in vegetation will help to evaluate the annual variability of phenology due to changing climate conditions [8,9]. In general, the normalized difference vegetation index (NDVI) has been used to estimate changes in vegetation. The NDVI is calculated using visible and near-infrared (NIR) bands [10] from Advanced Very-High-Resolution Radiometer (AVHRR), Terra Moderate Resolution Imaging Spectroradiometer (MODIS), and Landsat sensors. We used NDVI data derived from AVHRR, MODIS, and Landsat. Typically, positive NDVI values are associated with vegetated areas, while zero and negative values correspond to bare soil and water bodies [11]. Vegetation indices are utilized as a surrogate to estimate vegetation activity [10,12]. The bandwidths of the red and NIR bands were utilized to compute NDVI for the Landsat, MODIS and AVHRR sensors. The Landsat red band is between 620 and 690 nm, NIR (770 to 900 nm), and MODIS red (nominally 620 to 670 nm), and NIR (841 to 876 nm) bands are much narrower than the AVHRR red (585 to 680 nm) and NIR (730 to 980 nm) bands [13]. The NDVI is strongly associated with the biophysical properties of vegetation [14–16]. These biophysical characteristics include leaf area index (LAI), canopy height, or canopy composition [14–16]. The NDVI has been successfully used to monitor long-term vegetation dynamics [17–19], detecting vegetation and climate interactions [20,21], modeling the net primary productivity [22] and carbon estimation of terrestrial ecosystems [23].

Different global products, primarily based on AVHRR records, have been used for several regional to global scale vegetation research projects [24,25]. The NDVI from AVHRR is used to provide worldwide estimates of terrestrial primary production [24,25]. Currently, the National Aeronautics and Space Administration (NASA)-led Land Long Term Data Record (LTDR) version 5 (V5) is developing daily reflectance data from 1981 to present, which include an improved atmospheric correction scheme and Bidirectional Reflectance Distribution Function (BRDF) corrections [26]. The time series of AVHRR includes seven sensors on National Oceanic and Atmospheric Administration (NOAA), NOAA-07, NOAA-09, NOAA-11, NOAA-14, NOAA-16, NOAA-18, and NOAA-19. Several studies have focused on analyzing the time series of AVHRR NDVI and monitoring changes in vegetation phenology [2,27–30]. Long-term analysis of AVHRR NDVI has been intercompared with Landsat (Land use/Land cover) along with environmental variables, such as rainfall and air temperature, to understand the changes in biomass [2,31–34]. Time sequences of NDVI from Landsat have been employed to observe land cover changes. Several studies [35–38] have addressed the detection of disturbances, furnace, and logging events, whereas [39] monitored modifications in vegetation cover to evaluate the effects of changing grazing management practices. Several studies have compared AVHRR NDVI imagery to NDVI as derived from MODIS [40–45].

In this paper, we focus on the period of rehabilitation of the marshes (2002–2018) to estimate the increase in vegetation through the use of statistical analysis of the NDVI from the three different satellite sensors (Landsat, MODIS, and AVHRR). The NDVI derived from AVHRR LTDR will be

evaluated against Terra MODIS and Landsat 7 the Enhanced Thematic Mapper Plus (ETM+) data for the Mesopotamian marshlands in Iraq, using statistical analysis. In fact, there have been no previous studies to investigate temporal changes in vegetation coverage of the Iraqi marshlands using multiple sensors. In this study, we have examined the vegetation index of the study area using three different sensors that have different spatial resolution and temporal repeat. This paper investigates the utility of combining satellite data with low spatial resolution, frequent temporal repeat and long-term coverage with high spatial resolution data with low temporal repeat and comparable long-term coverage. The Landsat 7 ETM+ (30 m) and Terra MODIS NDVI (1 km) data have been resampled to the same spatial resolution as AVHRR LTDR (5 km). We examine the relationship between the NDVI values derived from the three sensors to understand the spatial patterns and the correlation of the NDVI values between the multiple sensors. We evaluate the accuracy of the time series trend of AVHRR NDVI, by comparison, the 1 km resolution Terra MODIS (MOD13A2) NDVI data, and 30 m Landsat 7 +ETM NDVI data.

2. Datasets and Methods

2.1. Study Area

The Mesopotamian marshlands are located in southern Iraq and partially in southwestern Iran, between 46.4° and 48.0° E longitude and 30.5° and 32.2° N latitude. The Mesopotamian marshes are freshwater wetlands that consist of shallow freshwater lakes, some of which are permanent lakes, while others are seasonal [2]. The marshes are the home of the oldest civilization and one of the largest freshwater marshes in the world [46,47]. The marshes lie in the spacious floodplain between the Euphrates and the Tigris rivers in the lower part of the Mesopotamian Basin (Figure 1).

The floodplains are an area of low elevation and have been created through the accumulation of alluvial materials carried by water runoff from upstream [48]. The marshes are an essential part of provincial biodiversity in the Middle East and serve as an important habitat for migratory birds and plant species, such as reeds. Additionally, the marshlands act as a natural wastewater treatment system for the water flowing from the Tigris and Euphrates rivers, as they filter out contaminants before the water reaches the Persian Gulf [2,3]. These marshlands are mainly composed of three distinct but closely located marshes—A-Hammar Marsh, the Central Marshes, and Al-Huwaiza Marsh. The main rivers feeding these marshes are the Euphrates, Tigris, and Karkha rivers. According to [49,50], the study area was located in an arid region, as determined by the annual rainfall and mean annual temperature. The mean annual rainfall and the average annual air temperature are less than 25 mm/year and 26.5 °C, respectively [2]. These marshlands have undergone several land use and land cover changes during the last decades [1,5,51].

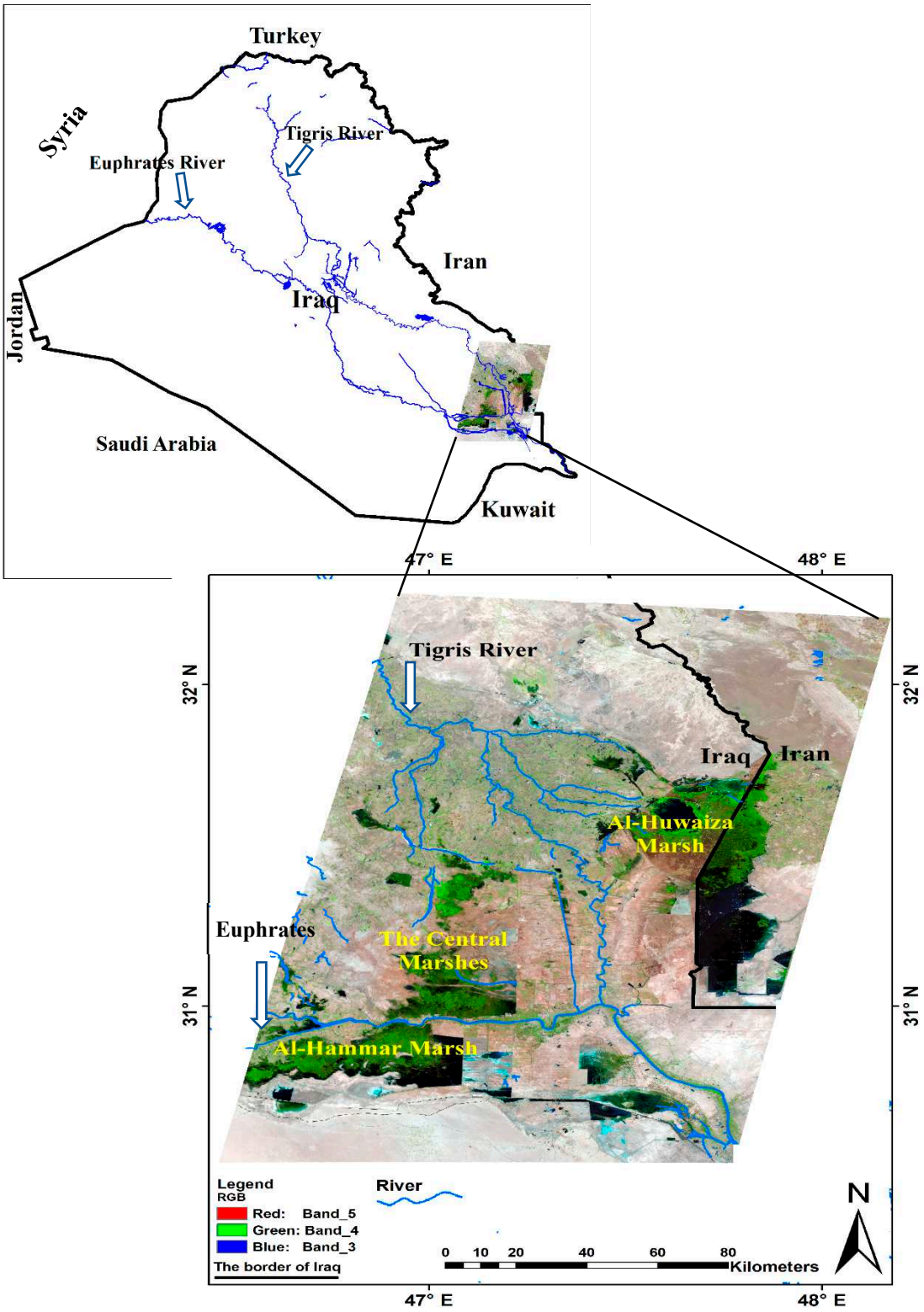

Figure 1. False color composite Enhanced Thematic Mapper Plus (ETM+) image for the Mesopotamian marshes for June 2018. Open water is shown in black and turquoise, vegetation is shown in dark and light green, and the barren area is represented in light brownish, white, and gray.

2.2. Data

2.2.1. AVHRR LTDR V5 Daily NDVI Product

AVHRR is onboard the National Oceanic and Atmospheric Administration (NOAA) polar-orbiting environmental satellites, which are used to calculate the NDVI [52,53]. The latest version (V5) products were made available (http://ltdr.nascom.nasa.gov) on 15 August 2017. The daily NDVI estimates are derived using daily surface reflectance data from the AVHRR instruments onboard the NOAA platforms. There are two spectral channels (Red and NIR) on the NOAA AVHRR sensor that are used to calculate the daily NDVI value. The data set used in this study was compiled from the NOAA-16, -18, and -19 sensors. The LTDR products from the NOAA AVHRR sensors are available at a spatial resolution of $0.05 \times 0.05°$ with daily temporal resolution. The LTDR NDVI products have been used to map vegetation area and burned areas [54–56] and assess droughts [57]. The NDVI has range from −1 to 1, where positive values represent vegetated areas, while negative NDVI values represent water bodies, snow, clouds, and non-vegetated surfaces [58,59] (Table 1).

Table 1. Data used in the present study.

Sensor/Model	Variable	Spatial Resolution	Temporal Resolution	Coverage
AVHRR [1]	NDVI [2]	0.05° (~5 km)	Daily	1981–Present
MODIS [3]	NDVI	1 km	16 Days	2002–Present
Landsat7	Bands 1–7	30 m	16 Days	1999–Present

[1] Advanced Very-High-Resolution Radiometer (AVHRR), [2] Normalized Difference Vegetation Index (NDVI), [3] Moderate Resolution Imaging Spectroradiometer (MODIS).

2.2.2. MODIS Data

In this study, we used the MOD13A2 Version 6 Vegetation Index (VI) values at 1 km spatial resolution [60] (https://lpdaac.usgs.gov/products/mod13a2v006/) (Table 1). MOD13A2 was processed from the MODIS L3 daily surface reflectance product (MOD09) that provided red and near-infrared surface reflectance, corrected for the effect of atmospheric gases, thin cirrus clouds, and aerosols. The atmospheric correction of MOD09 bands 1–7 had been based on the 6S radiative transfer model used to generate the surface reflectance [61]. The NOAA Center for Environment Prediction (NCEP) provided the surface pressure, ozone, and water vapor content for the atmospheric corrections for the MOD09 product [17].

2.2.3. Landsat

Landsat 7 ETM+ is the seventh satellite of the Landsat program. Launched on 15 April 1999, Landsat 7's goal is to refresh the global archive of satellite images, offering updated and cloud-free images. The Landsat 7 data products are generated at 30 m spatial resolution and 16 days repeat on a Universal Transverse Mercator (UTM) projection. The Landsat Program is managed, operated, and distributed by the United States Geological Survey (USGS). Landsat 4–7 Surface Reflectance data products are available via EarthExplorer. The USGS Earth Resources Observation and Science (EROS) Center Science Processing Architecture (ESPA) on-demand interface offers Landsat 4–5 Thematic Mapper (TM) and Landsat 7 ETM+ Surface Reflectance, in addition to Original Input Products and Metadata, TOA Reflectance, NDVI, Normalized Difference Moisture Index (NDMI), Normalized Burn Ratio (NBR), Normalized Burn Ratio 2 (NBR2), Soil Adjusted Vegetation Index (SAVI), Modified Soil Adjusted Vegetation Index (MSAVI), and Enhanced Vegetation Index (EVI) data products [62]. ESPA can be found at https://espa.cr.usgs.gov/. Additional information about ESPA's spectral indices and service processing options for Landsat 4–8 can be found in the Spectral Indices Product Guide and ESPA On-Demand Interface User Guide (https://landsat.usgs.gov/sites/default/files/documents/ledaps_product_guide.pdf) (Table 1).

2.2.4. Additional Data

The USGS Earth Explorer provides digital elevation model (DEM) elevations at a 30 m spatial resolution from the Space Shuttle Radar Topography Mission (SRTM). In this research, we used DEM data to examine the correlation between NDVI changes and elevation in the study area.

2.3. Methodology

The NDVI values were derived from the three sensors, AVHRR, MODIS, and Landsat 7 ETM+, for the Mesopotamian marshes corresponding to the maximum biomass period (June) over 17 years (2002–2018). According to [2], the growing season over the Mesopotamian marshes spans from April to August, with the maximum in the month of June. We used the month of June due to the minimum presence of clouds during the year. We mosaicked the Landsat images (Path 166 and Rows 38 and 39) of the study area for the month of June for the 2002–2018 period. Landsat path 166 and row 38 was centered at latitude 31°44′17.52″N and longitude 47°44′49.27″E. Path 166 and row 39 was centered at latitude 30°18′07.16″N and longitude 47°21057.1700E. As mentioned, the study area was covered by two Landsat ETM+ images (Path 166, Row 38, Path 166, Row 39). We used 34 images (two/year) and mosaicked them together. The MODIS and AVHRR were re-projected from the sinusoidal projection to the UTM projection, the same as the Landsat data. For the direct comparisons between LTDR AVHRR, Terra MODIS, and Landsat ETM+, NDVI data were resampled to the spatial resolution of AVHRR NDVI ($0.05 \times 0.05°$). The boxcar method was used for resampling when changing the pixel sizes. We took the average of all the 30 m or 1 km pixels for the NDVI from Landsat and MODIS, respectively, that fell inside a 5 km pixel of AVHRR as the 5 km pixel value. Spatial resolution alluded to the size of one pixel on the ground. In our examination, we utilized Landsat, MODIS, and AVHRR data that had 30 m, 1 km, and 5 km, respectively, that implied one pixel on an image corresponded to a square of 30 m by 30 m, 1 km by 1 km, and 5 km by 5 km on the ground, respectively. Sensors that have high spatial resolution cover a smaller area, while temporal repeat describes how frequently data for a region were gathered, also referred to as Revisit Time. The temporal repeat of the data was 16 days, 16 days, and daily for Landsat, MODIS, and AVHRR, respectively (Table 1). The three different sensors were intercompared over the 17-year period (2002–2018). We analyzed the NDVI time series by examining the linear trends over the 2002–2018 time period. The linear trend is one of the most essential descriptors of vegetation dynamics for time series, to determine an increase and/or decrease in vegetation by using linear regression analysis [8]. Simple linear regression was carried out for the NOAA AVHRR, MODIS, and Landsat ETM+ time collection, to observe the temporal changes in NDVI. The linear trend model was quantified using the p-value (tested for statistical significance at the confidence levels of 95% ($p < 0.05$) and 90% ($p < 0.1$)), the correlation coefficient (R^2) and the standard deviation (SD). We also used the DEM at 30 m to identify the relationship between elevation and changes in vegetation over the 17-year period.

3. Result

3.1. Time Series Analysis

For each pixel, we calculated the average NDVI over the 17-year period (2002–2018) for the three different sensors, at their original spatial resolution—5 km, 1 km, and 30 m for LTDR AVHRR, MODIS, and Landsat 7 ETM+, respectively (Figure 2). Figure 2 shows a good match, where NDVI values greater than 0.2 were mostly located in the northeast of the Al-Huwaiza marsh and the southwest and west parts of Al-Hammar and the Central marshes of the study area. If we examine Figure 2, we can see the "bulls-eye" feature on each of the images (for Landsat, MODIS, and AVHRR) that is present in the northeast corner of the area. There is a high vegetation area in the southwest corner of the area, which is seen in all three images. The only difference in both these features between the images is that in the AVHRR image the features are blurry (low resolution at 5 km) and in Landsat, the features are

sharp (high resolution at 30 m). MODIS displays the same feature with a resolution in between the two. Overall, the three datasets display similar average NDVI variability.

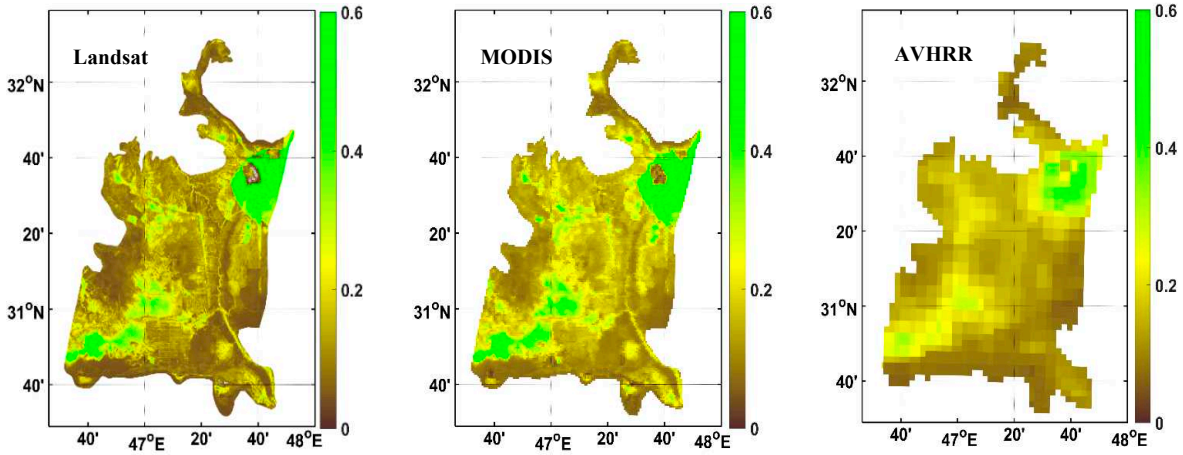

Figure 2. Average normalized difference vegetation index (NDVI) over the 17-year period (2002–2018) for three different sensors at their original spatial resolution—5 km, 1 km, and 30 m for Land Long Term Data Record (LTDR) Advanced Very-High-Resolution Radiometer (AVHRR), Moderate Resolution Imaging Spectroradiometer (MODIS) and Landsat 7 ETM+, respectively.

The Landsat and MODIS NDVI data were resampled to match the spatial resolution of the AVHRR NDVI (0.05 × 0.05°). We employed the boxcar method for this process. Each raster value was a temporal-average of 17 months (month of June). The peaks in the NDVI plots from the different sensors appeared at approximately the same time through the 17 years of overlap (Figure 3). Figure 3 shows that there is a good correspondence between the area-averaged NDVI derived from Landsat and AVHRR. In addition, the MODIS time series show a positive bias by about 0.02 relative to Landsat and AVHRR.

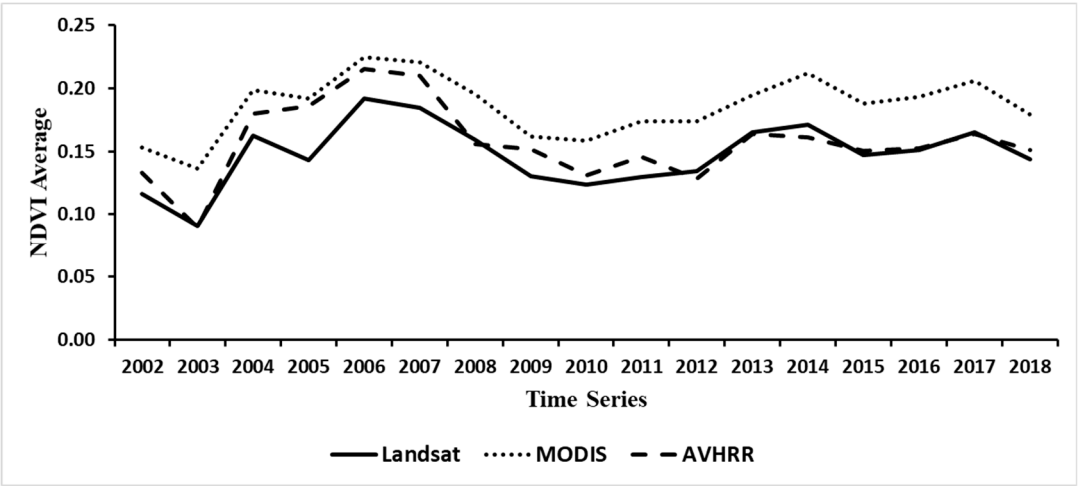

Figure 3. The time series of average NDVI from 2002 to 2018 for three different sensors at their original spatial resolution—5 km, 1 km, and 30 m for LTDR AVHRR, MODIS, and Landsat 7 ETM+, respectively.

There is a good spatial match after the resampling process (Figure 4). The same features discussed for Figure 2 can be seen in Figure 4. The only difference between the three images for these two features is that both the features appear sharper in the Landsat and MODIS as compared to AVHRR. This clearly demonstrates that the observation at a higher spatial resolution is important, and that averaging up (from 30 m and 1 km to 5 km) does not degrade the features displayed in the aggregated data.

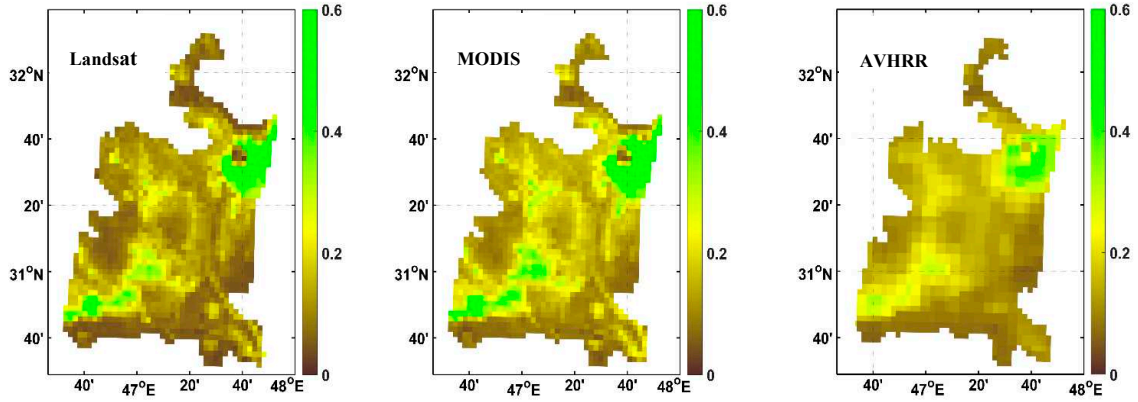

Figure 4. Average NDVI over the 17-year period (2002–2018) for Landsat 7 ETM+ and Terra MODIS NDVI resampled to the spatial resolution of AVHRR LTDR (5 km).

3.2. Comparison of Linear NDVI Trend Components

Pearson's correlation analysis was used for each pixel to investigate the consistency between the NDVI dataset derived from the LTDR AVHRR, Terra MODIS, and Landsat 7 ETM+ products from 2002 to 2018 (Figure 5). In particular, the Landsat NDVI–MODIS NDVI (Figure 5c) shows a higher correlation than the Landsat NDVI–AVHRR NDVI and MODIS NDVI–AVHRR NDVI (Figure 5a,b). The correlation coefficients between Landsat NDVI–AVHRR NDVI range from −0.2 to 0.6. About 10% of the area shows no significant agreement for Landsat and AVHRR NDVI. We can clearly see the lack of the dark red (correlation > 0.8) in Figure 5a (as compared to Figure 5c), signifying lower and some with no significant correlations between Landsat NDVI and AVHRR NDVI. The spatial pattern of the correlation between MODIS NDVI and AVHRR NDVI (Figure 5b) is quite similar to the spatial pattern of the correlation between Landsat NDVI and AVHRR NDVI (Figure 5a). The coefficient of correlation ranges between −0.3 and 0.6 (similar to Figure 5a). The correlation between Landsat NDVI and MODIS NDVI ranges between 0.4 and 0.9 (Figure 5c). This is much higher than the range of correlation between Landsat NDVI and AVHRR NDVI (Figure 5a) and MODIS NDVI and AVHRR NDVI (Figure 5b).

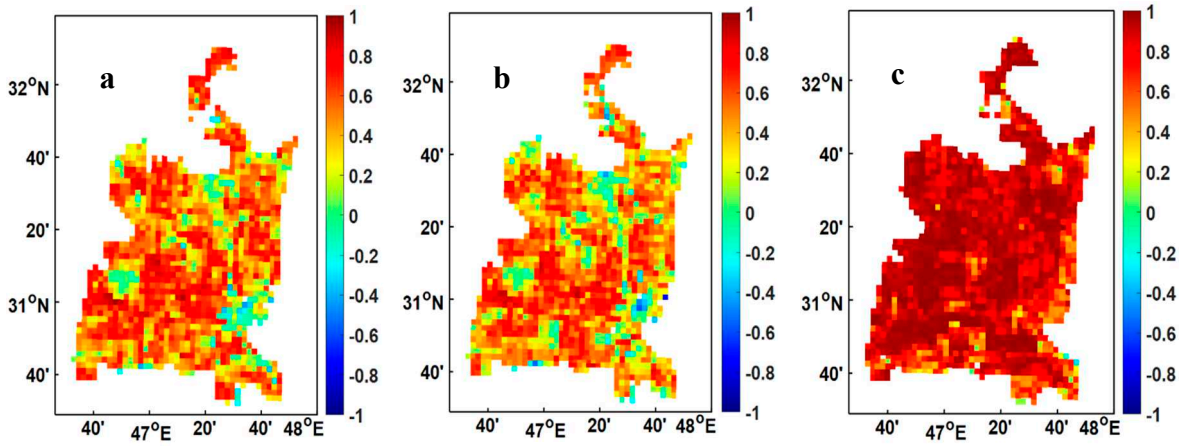

Figure 5. (**a**–**c**) Pearson's correlation analysis between NDVI from AVHRR, MODIS, and Landsat over 17 years (2002–2018). (**a**) Landsat–AVHRR (**b**) MODIS–AVHRR, and (**c**) Landsat–MODIS.

The most likely reason for the higher agreement between Landsat and MODIS is the closer spatial resolution of the two sensors (30 m and 1 km) as compared to MODIS and AVHRR (1 km and 5 km) or Landsat and AVHRR (30 m and 5 km). Additionally, the coefficient of determination (R^2) for the three different sensors over 17 years (2002–2018) shows a positive and high R^2 (Figure 6). Figure 6a shows a positive linear correlation between Landsat NDVI and AVHRR NDVI (R^2 = 0.79), Figure 6b represents

R^2 = 0.77 between MODIS NDVI and AVHRR NDVI, and Figure 6c shows R^2 = 0.96 between NDVI derived from Landsat 7 ETM+ and MOD13A2 V6. As expected from the correlation results displayed in Figure 5, the highest correlation is between Landsat NDVI and MODIS NDVI.

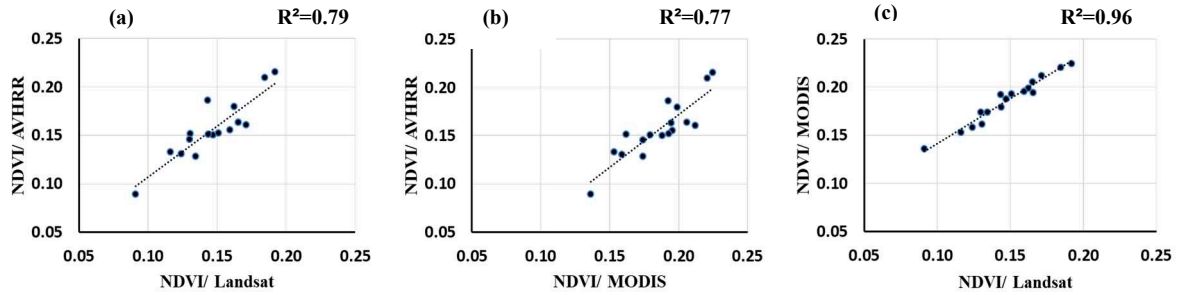

Figure 6. (**a**–**c**) Comparison of annual average NDVI values from the three different sensors over 17 years. (**a**) Landsat versus AVHRR, (**b**) MODIS versus AVHRR, and (**c**) Landsat versus MODIS.

We calculated the spatial standard deviation (SD) for each NDVI pixel of datasets at the LTDR AVHRR resolution over 17 years (Figure 7). The SD of the time series from the three sensors shows similar spatial patterns. We observed the same area of high standard deviation in the northeast portion of the study area as well as in the southwest portion (visible in the light blue color). Figure 7 shows that the standard deviation is generally less than 0.15 for all three sensors. This means that all sensors showed similar spatial variation of standard deviation NDVI around the average standard deviation of NDVI.

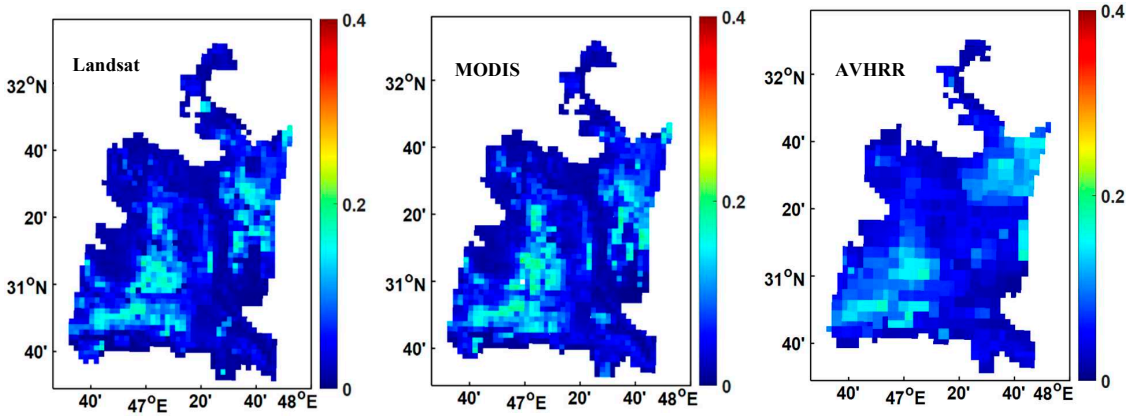

Figure 7. Temporal standard deviation for each pixel (2002–2018) for the three different sensors (AVHRR, MODIS, and Landsat).

The NDVI time series used to statistically analyze was based on linear regression, to identify the areas that showed a change in vegetation index over time. The temporal trend of vegetation greenness (NDVI) was measured using the slope. Figure 8 shows a computed linear slope (for each pixel) for the period from 2002 to 2018. This illustrates the locations of increase (positive slope) or decrease (negative slope) in vegetation. The color green (dark high, light low) (in Figure 8) represents an increase in NDVI, while light and dark brown colors represent the decline in NDVI. The range of increase and decrease in the slope of vegetation index is between −0.05 and 0.05. The green biomass (NDVI) of the Mesopotamian marshes over 17 years (2002–2018) increased in 33.2% of the total are, i.e., one-third of the area has a positive slope for the trend of the vegetation index. It can be seen from Figure 8 that the slope is slightly negative over most of the area (−0.002 to −0.05), indicating an overall slight decrease in the vegetation index over time. The areas of positive (green) and negative (brown) slopes were located in the same areas in each image, even though Landsat, MODIS, and AVHRR have different spatial resolutions (30 m, 1 km, and 5 km).

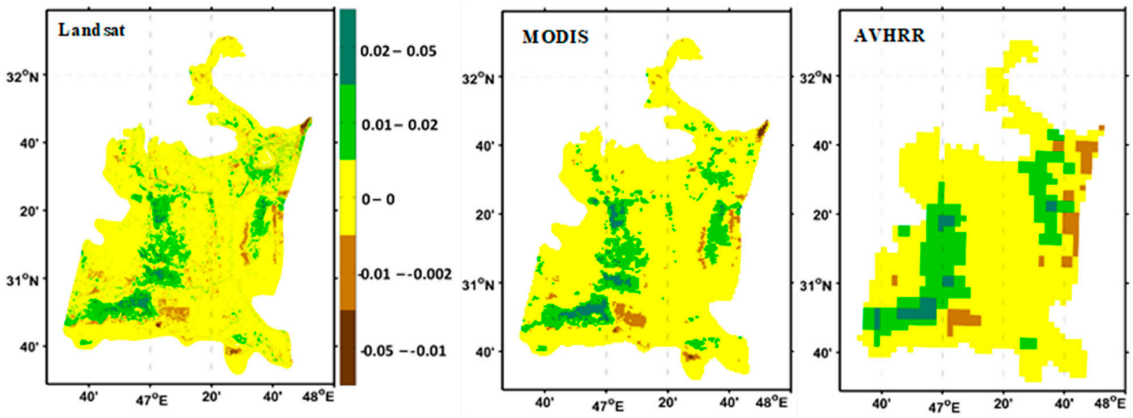

Figure 8. Linear slope of NDVI (AVHRR, MODIS, and Landsat) for each pixel over the period of 2002–2018, showing long-term trends of green biomass change in the Mesopotamian marshes.

According to the linear slope analysis, the three sensors are consistent. The reason for the increase in vegetation index in the west of Al-Hammar marsh, the northeast of Al-Huwaiza marsh, and the southern and middle parts of the Central marshes is due to the difference in elevation, where rivers and rainfall water that feed the marshes remain for a longer period due to the lower elevation. The increase in vegetation coverage is concentrated in the lowest elevations, which ranges between 0 and 6 m (Figure 9).

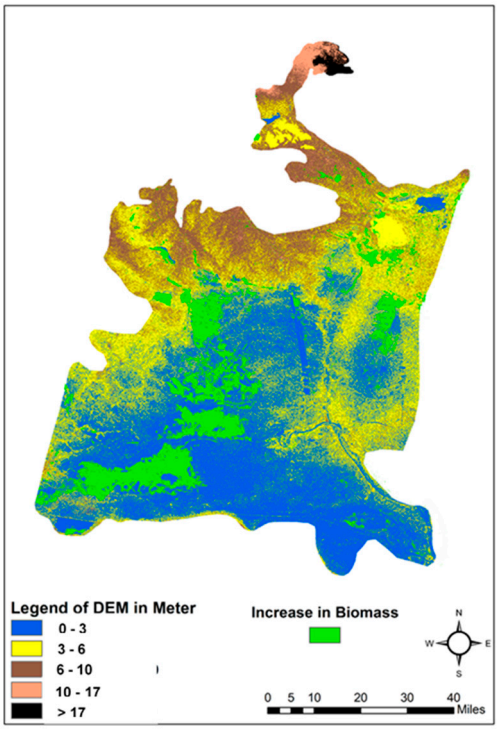

Figure 9. Combined digital elevation model (DEM) image (30 × 30 m) with the increase in vegetation coverage (from the linear slope of the NDVI).

These low elevation areas agree well with the areas of positive slope in the NDVI. Table 2 and Figure 10 show the inverse relationship between the increase in the green biomass over the time series and elevations. The increase in vegetation coverage, which is more than 2000 km^2, is concentrated in the lowlands (0–6 m) until it reaches as low as 0.4 km^2 in the highlands (>17 m).

Table 2. The correlation between the area of biomass (km^2) and elevation (m).

Elevation Range (m)	Area of Elevation in km^2	Area of Increase in Biomass Over 17 Years
0–3	3984.6	1615.7
3–6	3659.6	975.2
6–10	1279.4	412.8
10–17	97.6	5.8
>17	37.2	0.4

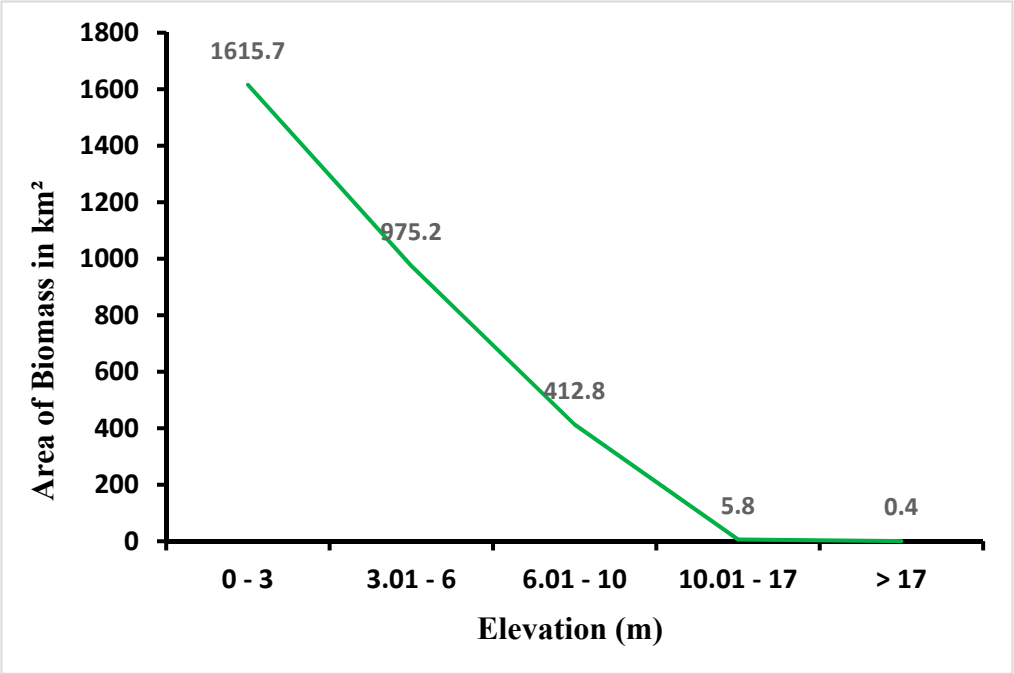

Figure 10. Correlation between vegetation (from linear slope of the NDVI) and elevation.

However, we tested the linear slope for statistical significance at the level of 95% ($p < 0.05$) and 90% ($p < 0.1$) (Figure 11). Figure 11 shows that the three datasets have a good match, where the three data clearly show the major areas are statistically significant, with $p < 0.05$ and $p < 0.1$.

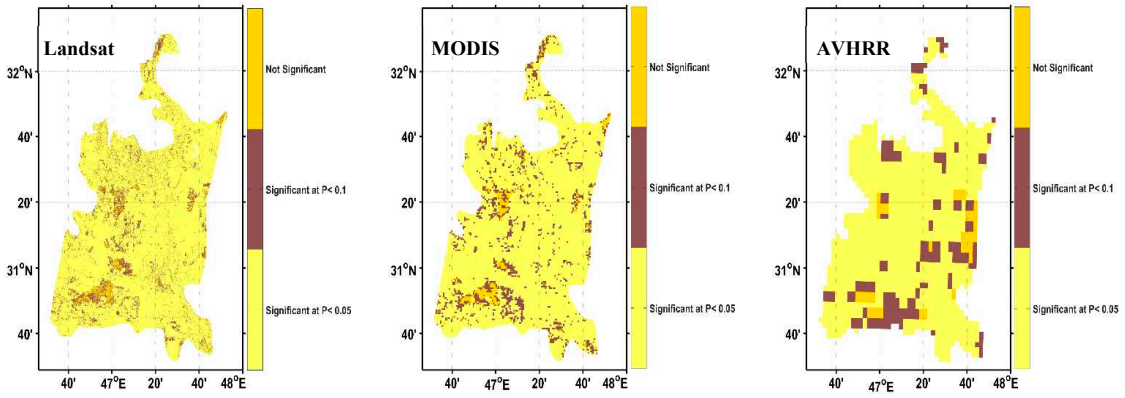

Figure 11. Pixel-based significance of linear slope over the period 2002–2018 for the Mesopotamian marshes from the three different sensors (AVHRR, MODIS, and Landsat).

4. Discussion

The Mesopotamian marshes had been subjected to drying operations almost for two decades (the late 1980s to late 2003) due to anthropogenic activities, through the construction of a series of dams

upstream of rivers in Turkey, Syria, Iran, and local canals and dams [2,5,63]. In late 2003, after the fall of Saddam's government, the marshes experienced re-flooding. In this paper, we have focused on the period of rehabilitation of the marshes (2002–2018) to examine the increase in vegetation index through the use of statistical analysis of the NDVI from the three different sensors (Landsat, MODIS, and AVHRR). We examined NDVI derived from the three different datasets—AVHRR LTDR V5, Terra MODIS, and Landsat 7 ETM+–for the Mesopotamian Marshes. The statistical analysis revealed that, although there are differences in spatial and temporal resolution between the three NDVI datasets, the overall trends and spatial variability in NDVI were similar over the 17-year period (2002–2018). The NDVI time series exhibited similar lowest and highest values of NDVI in 2003 and 2006, respectively (Figure 3). The coefficients of determination were positive between the three datasets. The linear correlations were 0.786, 0.774, and 0.959 between AVHR and Landsat, AVHRR and MODIS, and Landsat and MODIS, respectively. AVHRR has a much lower spatial resolution (5 km) as compared to MODIS (1 km) and Landsat (30 m). This is the reason for the low similarity. There have some previous studies that found similar results to ours. Gallo et al. [13], concluded that, despite the fact that distinctions exist in several factors which may impact the composite NDVI values, the 16-day composite NDVI values observed with the Terra and Aqua MODIS, and LTDR AVHRR, were comparable when examined over comparable time intervals and land cover. Bédard et al. [64], compared NDVI composites from NOAA AVHRR and Terra MODIS for pastureland in Alberta. They studied the statistical relationship between NDVI values derived from both sources and compared to pasture productivity field data. Correlation coefficients of 0.74 and 0.71 were obtained while correlating pasture productivity with NDVI composites from Terra MODIS and NOAA AVHRR, respectively. According to Brown et al. [12], the AVHRR NDVI dataset offers a bridge between the historical record and the newer satellite sensors, permitting an extension of the short records and assisting global change research that require the use of vegetation data. Tsuchiya et al. [65] studied the observations from three spectral bands (green, red, and near infrared) of the four sensors—Terra/ASTER, Terra/MODIS, NOAA/AVHRR, and Landsat/ETM+—and showed that the sensors were highly cross-correlated. We acknowledge that there are substantial differences between NDVI products, due to their spatial resolution and temporal repeat. However, we are interested in the differences in spatial patterns, as we have the high-resolution Landsat (30 m) at low temporal repeat (bi-weekly) and has been available for a long time period (1980s–present); the AVHRR has a low spatial resolution (5 km) but a good temporal repeat (daily), and has been available for a long time (1980s–present); and in between these two extremes is the MODIS, with moderate spatial resolution (1 km), good temporal repeat (daily), and a time interval of 20 years (2000–present). However, the standard deviations of the time series of NDVI that have been calculated from the three different sensors show a similar spatial pattern (Figure 7). The high values of standard deviation occur in the area that has a positive slope for the trend of vegetation index. The long-term trend of NDVI showed an increase in vegetation coverage in the western area of Al-Hammar marsh, the northeast of Al-Huwaiza marsh, and the south and middle parts of the Central marshes, in the three sensors. According to Guo et al. [17], the spatial distributions of the significantly positive trends of NDVI were similar between the two datasets (MODIS and LTDR AVHRR) for the Loess Plateau and Northeast Plain. The vegetation coverage of the marshes increased by 33.2% in the past 17 years (2002–2018). This increase in vegetation is due to the return of marsh dwellers, who demolished most of the canals and dams that had been built during Saddam's regime [1,2], which prevented water from reaching the marshes. Additionally, the increase in vegetation is linked to the difference in elevation. At low elevations (0–6 m), rivers and precipitation feed the marshes, which provides a favorable environment for plant growth.

5. Conclusion

In our recently published manuscript, Albarakat et al. [2], we calculated the statistical analysis (trend of NDVI) from 1982 when the Iraqi marshes were not affected by any anthropogenic activities. From 1982 to 1985, most of the Mesopotamian marshes were covered by vegetation and water bodies.

Between the late 1980s until 2003 the marshlands had been subjected to drying operations by the construction of the series of dams and canals that decreased the flow of the Tigris, Euphrates, and Karkha rivers through the marshlands. This led to the transformation of the marshes to barren land, and the vegetated areas significantly deteriorated compared to pre-drying years. During this research, we employed statistical analysis from 2002—the year which is widely considered to be the end of the drying operations. The Mesopotamian marshlands experienced re-flooding in late 2003, after the fall of Saddam's regime, due to the return of the marsh dwellers, who destroyed many of the canals and dams that had been previously built. In this study, we found the vegetation coverage of the marshes increased by 33.2% compared to 2002 (pre-re-flooding). However, as our analyses demonstrated, there was a similar performance of all three datasets examined here (AVHRR, MODIS, and Landsat). AVHRR can be considered an attractive source of information for studying long-term variations and trends in the land surface vegetation. In addition to AVHHR's long-term availability (almost four decades), AVHRR LTDR data are global and proven at a daily time repeat. The MODIS sensor temporal coverage is limited to less than 20 years (2000–present), and data are provided as 8- or 16-day composites. Landsat images are provided at 30 m spatial resolution and offer a long-term temporal record (30 years). However, the Landsat data are susceptible to cloud cover and only a few images are available per year (with a 20-day repeat visit). In this study, we found that the sensors are cross-correlated with high accuracy. This paper explores the utility of matching low spatial resolution with good temporal repeat and long-term coverage, and a high spatial resolution with low temporal repeat and similar long-term coverage. Finally, this study also proves that we can use the low-resolution AVHRR data for land cover change studies, as it shows a similar trend to the high-resolution Landsat over the same time period.

Author Contributions: Conceptualization, R.A., V.L.; Formal analysis, R.A. and V.L.; Methodology, R.A.; Project administration, R.A. and V.L.; Software, R.A.; Supervision, V.L.; Validation, V.L.; Writing original draft, R.A.; Writing–review & editing, V.L.

Funding: This research received no external funding.

Acknowledgments: The authors wish to thank the two anonymous reviewers and the editor for this manuscript for their helpful suggestions that have greatly improved the quality of this manuscript. We would like to thank Iliana E. Mladenova for her constructive comments. We are grateful to NASA and USGS for providing valuable datasets (AVHRR, MODIS, and Landsat data).

Conflicts of Interest: The authors declare no conflict of interest.

References

1. Richardson, C.J.; Hussain, N.A. Restoring the garden of Eden: An ecological assessment of the marshes of Iraq. *AIBS Bull.* **2006**, *56*, 477–489. [CrossRef]
2. Albarakat, R.; Lakshmi, V.; Tucker, C. Using Satellite Remote Sensing to Study the Impact of Climate and Anthropogenic Changes in the Mesopotamian Marshlands, Iraq. *Remote Sens.* **2018**, *10*, 1524. [CrossRef]
3. CIMI (Canada-Iraq Marshlands Initiative). *Managing for Change: The Present and Future State of the Marshes of Southern Iraq*; University of Victoria: Victoria, BC, Canada; Canadian International Development Agency: Gatineau, QC, Canada, 2010.
4. Douabul, A.A.Z.; Al-Saad, H.T.; Abdullah, D.S.; Salman, N.A. Designated protected Marsh within Mesopotamia: Water quality. *Am. J. Water Resour.* **2013**, *1*, 39–44.
5. Partow, H. *The Mesopotamian Marshlands: Demise of an Ecosystem*; Division of Early Warning and Assessment, United Nations Environment Programme; UNEP Publication: Nairobi, Kenya, 2001.
6. Maltby, E. *An Environmental and Ecological Study of the Marshlands of Mesopotamia Wetland Ecosystem*; AMAR Appeal Trust; University of Exeter: London, UK, 1994.
7. Vinez, M.; Leonard, S. *The Iraq Marshlands: The Loss of the Garden of Eden and Its People*; PLSI No. 3443; Illinois State University: Normal, IL, USA, 2010.
8. Stellmes, M.; Udelhoven, T.; Röder, A.; Sonnenschein, R.; Hill, J. Dryland observation at local and regional scale—Comparison of Landsat TM/ETM+ and NOAA AVHRR time series. *Remote Sens. Environ.* **2010**, *114*, 2111–2125. [CrossRef]

9. Turner, B.L.; Lambin, E.F.; Reenberg, A. The emergence of land change science for global environmental change and sustainability. *Proc. Natl. Acad. Sci. USA* **2007**, *104*, 20666–20671. [CrossRef]
10. Tucker, C.J. Red and photographic infrared linear combinations for monitoring vegetation. *Remote Sens. Environ.* **1979**, *8*, 127–150. [CrossRef]
11. Escuin, S.; Navarro, R.; Fernandez, P. Fire severity assessment by using NBR (Normalized Burn Ratio) and NDVI (Normalized Difference Vegetation Index) derived from LANDSAT TM/ETM images. *Int. J. Remote Sens.* **2008**, *29*, 1053–1073. [CrossRef]
12. Brown, M.E.; Pinzón, J.E.; Didan, K.; Morisette, J.T.; Tucker, C.J. Evaluation of the consistency of long-term NDVI time series derived from AVHRR, SPOT-vegetation, SeaWiFS, MODIS, and Landsat ETM+ sensors. *IEEE Trans. Geosci. Remote Sens.* **2006**, *44*, 1787–1793. [CrossRef]
13. Gallo, K.; Ji, L.; Reed, B.; Eidenshink, J.; Dwyer, J. Multi-platform comparisons of MODIS and AVHRR normalized difference vegetation index data. *Remote Sens. Environ.* **2005**, *99*, 221–231. [CrossRef]
14. Tong, A.; He, Y. Comparative analysis of SPOT, Landsat, MODIS, and AVHRR normalized difference vegetation index data on the estimation of leaf area index in a mixed grassland ecosystem. *J. Appl. Remote Sens.* **2013**, *7*, 073599. [CrossRef]
15. Goetz, S.J. Multi-sensor analysis of NDVI, surface temperature and biophysical variables at a mixed grassland site. *Int. J. Remote Sens.* **1997**, *18*, 71–94. [CrossRef]
16. Gianelle, D.; Vescovo, L.; Mason, F. Estimation of grassland biophysical parameters using hyperspectral reflectance for fire risk map prediction. *Int. J. Wildland Fire* **2009**, *18*, 815–824. [CrossRef]
17. Guo, X.; Zhang, H.; Wu, Z.; Zhao, J.; Zhang, Z. Comparison and evaluation of annual NDVI time series in China derived from the NOAA AVHRR LTDR and Terra MODIS mod13c1 products. *Sensors* **2017**, *17*, 1298.
18. Peng, J.; Liu, Z.; Liu, Y.; Wu, J.; Han, Y. Trend analysis of vegetation dynamics in Qinghai—Tibet Plateau using Hurst Exponent. *Ecol. Indic.* **2012**, *14*, 28–39. [CrossRef]
19. Zhao, J.; Wang, Y.; Hashimoto, H.; Melton, F.S.; Hiatt, S.H.; Zhang, H.; Nemani, R.R. The variation of land surface phenology from 1982 to 2006 along the Appalachian Trail. *IEEE Trans. Geosci. Remote Sens.* **2013**, *51*, 2087–2095. [CrossRef]
20. Piao, S.; Fang, J.; Zhou, L.; Guo, Q.; Henderson, M.; Ji, W.; Li, Y.; Tao, S. Interannual variations of monthly and seasonal normalized difference vegetation index (NDVI) in China from 1982 to 1999. *J. Geophys. Res. Atmos.* **2003**, *108*, 4401. [CrossRef]
21. Mao, D.; Wang, Z.; Luo, L.; Ren, C. Integrating AVHRR and MODIS data to monitor NDVI changes and their relationships with climatic parameters in Northeast China. *Int. J. Appl. Earth Obs. Geoinform.* **2012**, *18*, 528–536. [CrossRef]
22. Chirici, G.; Chiesi, M.; Corona, P.; Puletti, N.; Mura, M.; Maselli, F. Prediction of forest NPP in Italy by the combination of ground and remote sensing data. *Eur. J. For. Res.* **2015**, *134*, 453–467. [CrossRef]
23. Patil, V.; Singh, A.; Naik, N.; Unnikrishnan, S. Estimation of mangrove carbon stocks by applying remote sensing and GIS techniques. *Wetlands* **2015**, *35*, 695–707. [CrossRef]
24. Ruimy, A.; Saugier, B.; Dedier, G. Methodology for the estimation of terrestrial net primary production from remotely sensed data. *J. Geophys. Res.* **1994**, *99*, 5263–5283. [CrossRef]
25. Prince, S.D.; Goward, S.N. Global primary production: A remote sensing approach. *J. Biogeogr.* **1995**, *22*, 815–835. [CrossRef]
26. Pedelty, J.; Devadiga, S.; Masuoka, E.; Brown, M.; Pinzon, J.; Tucker, C.; Roy, D.P.; Ju, J.; Vermote, E.F.; Prince, S.D.; et al. Generating a long-term land data record from the AVHRR and MODIS Instruments. In Proceedings of the IEEE International Geoscience and Remote Sensing Symposium, Barcelona, Spain, 23–28 July 2007; pp. 1021–1025.
27. McCloy, K.R.; Los, S.; Lucht, W.; Højsgaard, S. A comparative analysis of three longterm NDVI data sets derived from AVHRR satellite data. *EARSeL eProc.* **2005**, *4*, 52–69.
28. Anyamba, A.; Tucker, C.J. Analysis of Sahelian vegetation dynamics using NOAA AVHRR NDVI data from 1981–2003. *J. Arid Environ.* **2005**, *63*, 596–614. [CrossRef]
29. Jeyaseelan, A.T.; Roy, P.S.; Young, S.S. Persistent changes in NDVI between 1982 and 2003 over India using AVHRR GIMMS (Global Inventory Modeling and Mapping Studies) data. *Int. J. Remote Sens.* **2007**, *28*, 4927–4946. [CrossRef]
30. Helldén, U.; Tottrup, C. Regional desertification: A global synthesis. *Global Planet Chang.* **2008**, *64*, 169–176. [CrossRef]

31. Xiao, J.; Moody, A. Geographical distribution of global greening trends and their climatic correlates: 1982–1998. *Int. J. Remote Sens.* **2005**, *26*, 2371–2390. [CrossRef]
32. Hickler, T.; Eklundh, L.; Seaquist, J.; Smith, B.; Ardö, J.; Olsson, L.; Sykes, M.T.; Sjostrom, M. Precipitation controls Sahel greening trend. *Geophys. Res. Lett.* **2005**, *32*, L21415. [CrossRef]
33. Herrmann, S.M.; Anyamba, A.; Tucker, C.J. Recent trends in vegetation dynamics in the African Sahel and their relationship to climate. *Global Environ. Chang.* **2005**, *15*, 394–404. [CrossRef]
34. Fensholt, R.; Rasmussen, K.; Nielsen, T.T.; Mbow, C. Evaluation of earth observation based long term vegetation trends—Intercomparing NDVI time series trend analysis consistency of Sahel from AVHRR GIMMS, Terra MODIS, and SPOT VGT data. *Remote Sens. Environ.* **2009**, *113*, 1886–1898. [CrossRef]
35. Viedma, O.; Moreno, J.M.; Rieiro, I. Interactions between land use/land cover change, forest fires and landscape structure in Sierra de Gredos (Central Spain). *Environ. Conserv.* **2006**, *33*, 212–222. [CrossRef]
36. Röder, A.; Udelhoven, T.; Hill, J.; del Barrio, G.; Tsiourlis, G. Trend analysis of Landsat-TM and ETM+ imagery to monitor grazing impact in a rangeland ecosystem in Northern Greece. *Remote Sens. Environ.* **2008**, *112*, 2863–2875. [CrossRef]
37. Röder, A.; Duguy, B.; Alloza, J.A.; Vallejo, R.; Hill, J. Using long time series of Landsat data to monitor fire events and post-fire dynamics and identify driving factors. *Remote Sens. Environ.* **2008**, *112*, 259–273. [CrossRef]
38. Kennedy, R.E.; Cohen, W.B.; Schroeder, T.A. Trajectory-based change detection for automated characterization of forest disturbance dynamics. *Remote Sens. Environ.* **2007**, *110*, 370–386. [CrossRef]
39. Hostert, P.; Röder, A.; Hill, J. Coupling spectral unmixing and trend analysis for monitoring of long-term vegetation dynamics in Mediterranean rangelands. *Remote Sens. Environ.* **2003**, *87*, 183–197. [CrossRef]
40. Fensholt, R. Earth observation of vegetation status in the Sahelian and Sudanian West Africa: Comparison of Terra MODIS and NOAA AVHRR satellite data. *Int. J. Remote Sens.* **2004**, *25*, 1641–1659. [CrossRef]
41. Huete, A.R.; Didan, K.; Miura, T.; Rodriguez, E.P.; Gao, X.; Ferreira, L.G. Overview of the radiometric and biophysical performance of the MODIS vegetation indices. *Remote Sens. Environ.* **2002**, *83*, 195–213. [CrossRef]
42. Kawamura, K.; Akiyama, T.; Yokota, H.; Tsutsumi, M.; Yasuda, T.; Watanabe, O.; Wang, S. Comparing MODIS vegetation indices with AVHRR NDVI for monitoring the forage quantity and quality in Inner Mongolia grassland, China. *Grassl. Sci.* **2005**, *51*, 33–40. [CrossRef]
43. Tarnavsky, E.; Garrigues, S.; Brown, M.E. Multiscale geostatistical analysis of AVHRR, SPOT-VGT, and MODIS global NDVI products. *Remote Sens. Environ.* **2008**, *112*, 535–549. [CrossRef]
44. Tucker, C.J.; Pinzon, J.E.; Brown, M.E.; Slayback, D.A.; Pak, E.W.; Mahoney, R.; Vermote, E.F.; Saleous, N.E. An extended AVHRR 8-km NDVI dataset compatible with MODIS and SPOT vegetation NDVI data. *Int. J. Remote Sens.* **2005**, *2*, 4485–4498. [CrossRef]
45. Venturini, V.; Bisht, G.; Islam, S.; Jiang, L. Comparison of evaporative fractions estimated from AVHRR and MODIS sensors over South Florida. *Remote Sens. Environ.* **2004**, *93*, 77–86. [CrossRef]
46. Maxwell, G. *People of the Reeds*; ASIN: B0007DMCTC; Harper: New York, NY, USA, 1957; 223p.
47. Young, G. *Return to the Marshes: Life with the Marsh Arabs of Iraq*; Collins: London, UK, 1977; 224p, ISBN 9780571280971.
48. Lubinski, B.J.; Jackson, J.R.; Eggleton, M.A. Relationships between floodplain lake fish communities and environmental variables in a large river-floodplain ecosystem. *Trans. Am. Fish Soc.* **2008**, *137*, 895–908. [CrossRef]
49. Peltier, L.C. The geographic cycle in periglacial regions as it is related to climatic geomorphology. *Ann. Assoc. Am. Geogr.* **1950**, *40*, 214–236. [CrossRef]
50. Fookes, P.G.; Dearman, W.R.; Franklin, J.A. Some engineering aspects of rock weathering with field examples from Dartmoor and elsewhere. *Q. J. Eng. Geol. Hydrogeol.* **1971**, *4*, 139–185. [CrossRef]
51. Richardson, C.J. *The Status of Mesopotamian Marsh Restoration in Iraq: A Case Study of Transboundary Water Issues and Internal Water Allocation Problems*; Towards New Solutions in Managing Environmental Crisis; University of Helsinki: Helsinki, Finland, 2010.
52. Rogan, J.; Franklin, J.; Roberts, D.A. A comparison of methods for monitoring multitemporal vegetation change using thematic mapper imagery. *Remote Sens. Environ.* **2002**, *80*, 143–156. [CrossRef]
53. Finlayson, C.; Davidson, N.; Spiers, A.; Stevenson, N. Global wetland inventory—Current status and future priorities. *Mar. Freshw. Res.* **1999**, *50*, 717–727. [CrossRef]

54. Moreno Ruiz, J.A.; Riaño, D.; Arbelo, M.; French, N.H.F.; Ustin, S.L.; Whiting, M.L. Burned area mapping time series in Canada (1984–1999) from NOAA-AVHRR LTDR: A comparison with other remote sensing products and fire perimeters. *Remote Sens. Environ.* **2012**, *117*, 407–414. [CrossRef]
55. Moreno-Ruiz, J.A.; Riano, D.; Garcia-Lazaro, J.R.; Ustin, S.L. Intercomparison of AVHRR PAL and LTDR version 2 long-term data sets for Africa from 1982 to 2000 and its impact on mapping burned area. *IEEE Geosci. Remote Sens. Lett.* **2009**, *6*, 738–742. [CrossRef]
56. Ruiz, J.A.M.; Lázaro, J.R.G.; Cano, I.D.Á.; Leal, P.H. Burned area mapping in the North American boreal forest using Terra-MODIS LTDR (2001–2011): A comparison with the MCD45A1, MCD64A1, and BA GEOLAND-2 products. *Remote Sens.* **2014**, *6*, 815–840. [CrossRef]
57. Ghulam, A.; Kasimu, A.; Kusky, T. Normalization of modified perpendicular drought index using LTDR and GIMMS dataset for drought assessment in the United States. In Proceedings of the IEEE International Geoscience and Remote Sensing Symposium, Boston, MA, USA, 7–11 July 2008; pp. III-856–III-859.
58. Vermote, E. Climate Algorithm Theoretical Basis Document (C-ATBD): AVHRR Land Bundle-Surface Reflectance and Normalized Difference Vegetation Index. 2013.f3. Available online: https://www.ncdc.noaa.gov (accessed on 20 November 2018).
59. Holben, B.N. Characteristics of maximum-value composite images from temporal avhrr data. *Int. J. Remote Sens.* **1986**, *7*, 1417–1434. [CrossRef]
60. Huete, A.; Didan, K.; van Leeuwen, W.; Miura, T.; Glenn, E. MODIS vegetation indices. In *Land Remote Sensing and Global Environmental Change*; Springer: New York, NY, USA, 2010; pp. 579–602.
61. Vermote, E.F.; El Saleous, N.Z.; Justice, C.O. Atmospheric correction of MODIS data in the visible to middle infrared: First results. *Remote Sens. Environ.* **2002**, *83*, 97–111. [CrossRef]
62. NASA ESPA. Landsat 7 Etm+ Level 2 Landsat 4-7 Surface Reflectance (Ledaps) Product GUIDE USGS Earth Resources Observation and Science (EROS) Center, Sioux Falls, South Dakota. 2018. Available online: https://lpdaac.usgs.gov (accessed on 8 September 2018).
63. Altinbilek, D. Development and management of the Euphrates–Tigris basin. *Int. J. Water Resour. Dev.* **2004**, *20*, 15–33. [CrossRef]
64. Bédard, F.; Crump, S.; Gaudreau, J. A comparison between Terra MODIS and NOAA AVHRR NDVI satellite image composites for the monitoring of natural grassland conditions in Alberta, Canada. *Can. J. Remote Sen.* **2006**, *32*, 44–50. [CrossRef]
65. Tsuchiya, K.; Kaneko, M.; Sung, S.J. Comparison of image data acquired with AVHRR, MODIS, ETM+, and ASTER over Hokkaido, Japan. *Adv. Space Res.* **2003**, *32*, 2211–2216.